

# Study and analysis of porosity distribution effects on the buckling behavior of functionally graded plates subjected to diverse thermal loading

Abdelhak Zohra<sup>2,3</sup>, Benferhat Rabia<sup>1,3</sup> and Hassaine Daouadji Tahar<sup>\*1,3</sup>

<sup>1</sup>Civil Engineering Department, University of Tiaret, Algeria

<sup>2</sup>Civil Engineering Department, University Center of Relizane, Algeria

<sup>3</sup>Laboratory of Geomatics and Sustainable Development, University of Tiaret, Algeria

(Received September 6, 2023, Revised October 9, 2023, Accepted October 29, 2023)

**Abstract.** This paper introduces an improved shear deformation theory for analyzing the buckling behavior of functionally graded plates subjected to varying temperatures. The transverse shear strain functions employed satisfy the stress-free condition on the plate surfaces without requiring shear correction factors. The material properties and thermal expansion coefficient of the porous functionally graded plate are assumed temperature-dependent and exhibit continuous variation throughout the thickness, following a modified power-law distribution based on the volume fractions of the constituents. Moreover, the study considers the influence of porosity distribution on the buckling of the functionally graded plates. Thermal loads are assumed to have uniform, linear, and nonlinear distributions through the thickness. The obtained results, considering the effect of porosity distribution, are compared with alternative solutions available in the existing literature. Additionally, this study provides comprehensive discussions on the influence of various parameters, emphasizing the importance of accounting for the porosity distribution in the buckling analysis of functionally graded plates.

**Keywords:** buckling behavior; FGM plate; porosity distribution; thermal expansion

---

## 1. Introduction

The emergence of Functionally Graded Materials (FGMs) has revolutionized the field of composites. Unlike traditional composite materials, FGMs offer a seamless and continuous variation between different materials, eliminating stress concentration and the risk of failure. Proposed in the early 1980s by Japanese scientists to address delamination in reusable rocket engines, FGMs allow tailored material gradation along preferred directions, resulting in distinct and desired properties. These advanced composites are highly versatile and well suited for various engineering applications, offering superior performance in challenging environments with varying thermal and mechanical conditions. FGMs represent a significant advancement, empowering engineers to design materials with enhanced resilience and efficiency (Tounsi *et al.* 2023,

---

\*Corresponding author, Ph.D., E-mail: daouadjitahar@gmail.com

HassaineDaouadji *et al.* 2021e, Fan *et al.* 2021, Radwan 2017, Wang *et al.* 2021, Abdelhak *et al.* 2023, Bouakaz *et al.* 2014, Rabahi *et al.* 2019, Rabahi *et al.* 2023, Chergui *et al.* 2019, Hamrat *et al.* 2020, Ben Henni *et al.* 2021, Bensatallah *et al.* 2023, Haytham *et al.* 2023a, Haytham *et al.* 2023b, Kablia *et al.* 2023, Kablia *et al.* 20022, Tounsi *et al.* 2008, Hassaine Daouadji 2017, Benferhat *et al.* 2018, Hassaine Daouadji *et al.* 2022, Rabia *et al.* 2019, Rabahi *et al.* 2022a, Tlidji *et al.* 2022, Hussein 2021, Bouiadjra *et al.* 2012).

The exploration of the buckling behavior in Functionally Graded Material plates holds substantial importance within a wide range of industrial domains, spanning aerospace, civil engineering, and the fabrication of biomedical devices. Due to their exceptional properties, numerous researchers have dedicated their endeavors to the analysis of buckling in FGM materials. In their work, Yassir *et al.* (2021) introduced an advanced finite element model for analyzing the buckling and post-buckling behavior of functionally graded material plates. Their investigation encompassed varying load conditions and solicitations applied to FGM plates. Adnan *et al.* (2021) conducted a series of analyses to explore the buckling tendencies of thin plates made of Functionally Graded Material featuring diverse circular cutout configurations. The computational simulation employed the Finite Element (FE) software Abaqus. Ramu *et al.* (2014) delved into the buckling analysis of rectangular FGM plates using classical plate theory (CPT). They investigated uniaxial and biaxial compression loads, along with simply supported boundary conditions, on these plates. Souhit *et al.* (2021) examined the thermomechanical-buckling response of skewed functionally graded plates subjected to varying thermal loads. This study utilized the finite element method based on the Love-Kirchhoff assumptions (Rabahi *et al.* 2021b, Hassaine Daouadji 2013). Bouaza *et al.* (2009) explored thermal buckling analyses of S-FGM structures by employing a first order shear deformation theory. The thermal buckling behaviors were analyzed under uniform, linear, and sinusoidal temperature distributions across the material thickness (Benferhat *et al.* 2019, Rabahi *et al.* 2021a, Hassaine Daouadji *et al.* 2021d). Think *et al.* (2016) introduced a novel eight-unknown higher-order shear deformation theory to investigate the buckling and free vibration characteristics of functionally graded material plates. Their theory is rooted in a comprehensive twelve-unknown higher-order shear deformation theory that simultaneously ensures zero transverse shear stress at the upper and lower surfaces of the FG plates. SiddaReddy *et al.* (2013) presented analytical formulations and solutions for the buckling analysis of simply supported functionally graded plates using a higher-order shear deformation theory (HSDT), all without imposing zero transverse shear stresses on the upper and lower plate surfaces. Thus, several researchers have studied this approach well (Hassaine Daouadji *et al.* 2019, Benferhat *et al.* 2021a, Rabahi *et al.* 2022b, Hassaine Daouadji *et al.* 2021b, Rabahi *et al.* 2020, Rabia *et al.* 2020, Hassaine Daouadji *et al.* 2020, Benferhat *et al.* 2021b).

Research studies on the effect of porosity on the buckling of FGM plates and beams play a crucial role in advancing our understanding of the mechanical and thermal behaviors of these complex materials. Kumar *et al.* (2023) explored the buckling behavior of porous plates composed of functionally graded materials subjected to uniaxial and biaxial loading under diverse boundary conditions. In a similar vein, Chen *et al.* (2015) investigated the elastic buckling and static bending characteristics of shear deformable functionally graded porous beams, employing the Timoshenko beam theory. Moving forward, Zenkour *et al.* (2022) delved into the buckling response of functionally graded porous plates, utilizing a quasi-3D refined theory that accounts for thickness stretching effects. This comprehensive theory introduced three distinct models for FG porous plates: an isotropic FG porous plate, FG skins encompassing a homogeneous core, and an FG core accompanied by homogeneous skins. Addressing a related aspect, Bekki *et al.* (2021) analyzed the

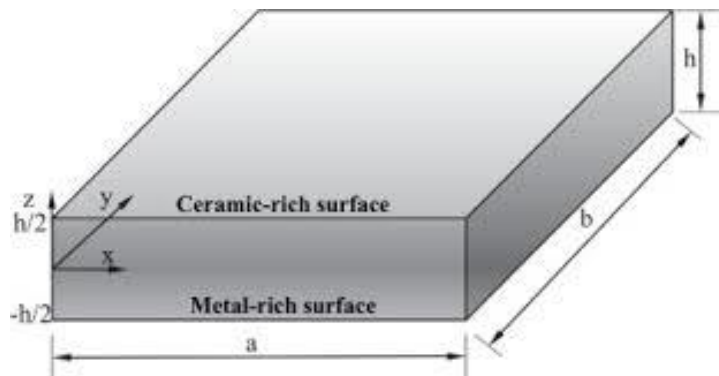


Fig. 1 FGM plate in the global coordinate system

influence of porosity on the buckling of functionally graded sandwich plates under thermal loading that extends throughout the thickness of the plate. Their investigation employed the four-variable refined plate theory and encompassed various types of functionally graded material sandwich plates, as well as diverse boundary conditions, to highlight the impact of transverse shear (Benferhat *et al.* 2023, Rabia *et al.* 2016, Hassaine Daouadji *et al.* 2021a, Hassaine Daouadji *et al.* 2021c, Rabahi *et al.* 2021c, Rabahi *et al.* 2021d).

From the above literature, it is found that the effect of distribution shape of porosity on the buckling of FGM plate subjected to varying temperatures has received few attentions. Hence, the present work has been done on the above limitations to bring the completeness of analysis on FGM plates. This study aims to develop analytical formulations and solutions for assessing the buckling behavior of functionally graded plates while considering the impact of porosity. The analysis employs a higher-order shear deformation theory (HSDT) that does not enforce zero transverse shear stress on the top and bottom surfaces of the plate, thereby eliminating the need for a shear correction factor. The material composition of the plate varies across its thickness, resulting in a unique distribution of porosity. By applying the principle of virtual work, the governing equations of the plate are derived. Closed-form solutions for FGPs are obtained using Navier's technique and solving the eigenvalue equation. In order to validate the accuracy of the proposed theory in predicting the critical buckling loads of FG plates, the obtained results are compared with findings from previous research studies. With the accuracy of the FG plate results confirmed, the study proceeds to analyze how various factors influence the critical buckling loads. These factors include the shape of the porosity distribution, side-to-thickness ratios, aspect ratios, modulus ratios, and volume fraction exponent.

## 2. Theoretical formulation

### 2.1 Displacement field and strains

Consider a plate with a total thickness represented as  $h$ . This plate is fabricated using a material that demonstrates functional grading throughout the thickness. This material possesses uniform properties in all directions, while the grading exclusively occurs along the thickness dimension of the plate. The  $xy$  plane is taken to be the undeformed mid plane of the plate with the  $z$  axis

positive upward from the mid plane (Fig. 1).

The displacement field of this theory can be formulated as follows

$$\begin{aligned} u(x, y, z, t) &= u_0(x, y, t) - z \frac{\partial w_b}{\partial x} - \frac{1}{n} \left(\frac{z}{h}\right)^{n-1} z^n \frac{\partial w_s}{\partial x} \\ v(x, y, z, t) &= v_0(x, y, t) - z \frac{\partial w_b}{\partial y} - \frac{1}{n} \left(\frac{z}{h}\right)^{n-1} z^n \frac{\partial w_s}{\partial y} \quad n = 3, 5, 7, 9, \dots \\ w(x, y, z, t) &= w_b(x, y, t) + w_s(x, y, t) \end{aligned} \quad (1)$$

The mid-plane displacements of the plate in the  $x$  and  $y$  directions are denoted as  $u_0$  and  $v_0$  respectively. Meanwhile,  $w_b$  represents the bending component, and  $w_s$  signifies the shear component of transverse displacement.

The equations describing the strain-displacement relationship, following the non-linear von Karman formulation, can be stated as follows

$$\begin{Bmatrix} \varepsilon_x \\ \varepsilon_y \\ \gamma_{xy} \end{Bmatrix} = \begin{Bmatrix} \varepsilon_x^0 \\ \varepsilon_y^0 \\ \gamma_{xy}^0 \end{Bmatrix} + z \begin{Bmatrix} k_x^b \\ k_y^b \\ k_{xy}^b \end{Bmatrix} + f(z) \begin{Bmatrix} k_x^s \\ k_y^s \\ k_{xy}^s \end{Bmatrix}, \quad (2a)$$

$$\begin{Bmatrix} \gamma_{yz} \\ \gamma_{xz} \end{Bmatrix} = g(z) \begin{Bmatrix} \gamma_{yz}^s \\ \gamma_{xz}^s \end{Bmatrix}, \quad (2b)$$

$$\varepsilon_z = 0 \quad (2c)$$

$$\text{Where: } \begin{Bmatrix} \varepsilon_x^0 \\ \varepsilon_y^0 \\ \gamma_{xy}^0 \end{Bmatrix} = \left\{ \begin{array}{l} \frac{\partial u_0}{\partial x} + \frac{1}{2} \left( \frac{\partial w_b}{\partial x} + \frac{\partial w_s}{\partial x} \right)^2 \\ \frac{\partial v_0}{\partial y} + \frac{1}{2} \left( \frac{\partial w_b}{\partial y} + \frac{\partial w_s}{\partial y} \right)^2 \\ \frac{\partial u_0}{\partial y} + \frac{\partial v_0}{\partial x} + \left( \frac{\partial w_b}{\partial x} + \frac{\partial w_s}{\partial x} \right) \left( \frac{\partial w_b}{\partial y} + \frac{\partial w_s}{\partial y} \right) \end{array} \right\}, \quad (3a)$$

$$\begin{Bmatrix} k_x^b \\ k_y^b \\ k_{xy}^b \end{Bmatrix} = \begin{Bmatrix} -\frac{\partial^2 w_b}{\partial x^2} \\ -\frac{\partial^2 w_b}{\partial y^2} \\ -2 \frac{\partial^2 w_b}{\partial x \partial y} \end{Bmatrix}, \quad (3b)$$

$$\begin{Bmatrix} k_x^s \\ k_y^s \\ k_{xy}^s \end{Bmatrix} = \begin{Bmatrix} -\frac{\partial^2 w_s}{\partial x^2} \\ -\frac{\partial^2 w_s}{\partial y^2} \\ -2 \frac{\partial^2 w_s}{\partial x \partial y} \end{Bmatrix}, \quad (3c)$$

$$\begin{Bmatrix} \gamma_{yz}^s \\ \gamma_{xz}^s \end{Bmatrix} = \begin{Bmatrix} \frac{\partial w_s}{\partial y} \\ \frac{\partial w_s}{\partial x} \end{Bmatrix}, \quad (3d)$$

$$f = \frac{z^n \left(\frac{z}{h}\right)^{n-1}}{n}; \quad g = 1 - \frac{z^n \left(\frac{z}{h}\right)^{n-1}}{z} \quad (3e)$$

### 2.2 Constitutive relations

Analyze a functionally graded plate composed of a combination of ceramics and metals. This plate subjected a thermal load denoted as  $T(x, y, z)$ . It is assumed that the material properties of the functionally graded material (FGM) undergo changes across the thickness of the plate. The variation in material characteristics can be formulated as follows

$$P = P_m \left( V_m - \frac{\beta}{2} \right) + P_c \left( V_c - \frac{\beta}{2} \right) \quad (4a)$$

Distribution shape of porosity	The expression of the young's modulus $E(z)$ and the coefficient of thermal expansion $\alpha(z)$ of each form of porosity distribution
Homogeneous porosity distribution	$E(z) = (e_c - e_m) * \left( \left( \frac{z}{h} + 0.5 \right) \right)^k + e_m - (e_c + e_m) * \frac{\beta}{2}$ (4b)
	$\alpha(z) = (\alpha_c - \alpha_m) * \left( \left( \frac{z}{h} + 0.5 \right) \right)^k + \alpha_m - (\alpha_c + \alpha_m) * \frac{\beta}{2}$ (4c)
X shape distribution of porosity	$E(z) = (e_c - e_m) * \left( \left( \frac{z}{h} + 0.5 \right) \right)^k + e_m - (e_c + e_m) * \frac{\beta}{2} * 2 * \frac{z}{h}$ (4d)
	$\alpha(z) = (\alpha_c - \alpha_m) * \left( \left( \frac{z}{h} + 0.5 \right) \right)^k + \alpha_m - (\alpha_c + \alpha_m) * \frac{\beta}{2} * 2 * \frac{z}{h}$ (4e)
O shape distribution of porosity	$E(z) = (e_c - e_m) * \left( \left( \frac{z}{h} + 0.5 \right) \right)^k + e_m - (e_c + e_m) * \frac{\beta}{2} * \left( 1 - 2 * \frac{z}{h} \right)$ (4f)
	$\alpha(z) = (\alpha_c - \alpha_m) * \left( \left( \frac{z}{h} + 0.5 \right) \right)^k + \alpha_m - (\alpha_c + \alpha_m) * \frac{\beta}{2} * \left( 1 - 2 * \frac{z}{h} \right)$ (4g)
V shape distribution of porosity	$E(z) = (e_c - e_m) * \left( \left( \frac{z}{h} + 0.5 \right) \right)^k + e_m - (e_c + e_m) * \frac{\beta}{2} * \left( \frac{1}{2} + \frac{z}{h} \right)$ (4h)
	$\alpha(z) = (\alpha_c - \alpha_m) * \left( \left( \frac{z}{h} + 0.5 \right) \right)^k + \alpha_m - (\alpha_c + \alpha_m) * \frac{\beta}{2} * \left( \frac{1}{2} + \frac{z}{h} \right)$ (4i)
$\Lambda$ shape distribution of porosity	$E(z) = (e_c - e_m) * \left( \left( \frac{z}{h} + 0.5 \right) \right)^k + e_m - (e_c + e_m) * \frac{\beta}{2} * \left( \frac{1}{2} - \frac{z}{h} \right)$ (4j)
	$\alpha(z) = (\alpha_c - \alpha_m) * \left( \left( \frac{z}{h} + 0.5 \right) \right)^k + \alpha_m - (\alpha_c + \alpha_m) * \frac{\beta}{2} * \left( \frac{1}{2} - \frac{z}{h} \right)$ (4k)

Where,  $\beta$ : volume fraction of porosity

$P$  symbolizes a general material property, such as modulus, while  $P_t$  and  $P_b$  represent the respective properties of the upper and lower surfaces of the plate. Additionally,  $V_t$  in Eq. (4) signifies the volume fraction of the upper surface constituent, which adheres to a straightforward power-law function

$$V_t = \left( \frac{z}{h} + \frac{1}{2} \right)^k \quad (5)$$

Here,  $k$  ( $0 \leq k \leq \infty$ ) serves as a parameter influencing the material variation pattern across the

thickness. In this context, we consider that the moduli  $E$ ,  $G$ , and the coefficient of thermal expansion  $\alpha$  vary as defined in Eq. (4), while the Poisson's ratio  $\nu$  is held constant.

The linear relationships governing the constitutive behavior are as follows

$$\begin{Bmatrix} \sigma_x \\ \sigma_y \\ \tau_{xy} \end{Bmatrix} = \begin{bmatrix} Q_{11} & Q_{12} & 0 \\ Q_{12} & Q_{22} & 0 \\ 0 & 0 & Q_{66} \end{bmatrix} \begin{Bmatrix} \varepsilon_x - \alpha T \\ \varepsilon_y - \alpha T \\ \gamma_{xy} \end{Bmatrix} \quad (6a)$$

$$\text{and } \begin{Bmatrix} \tau_{yz} \\ \tau_{zx} \end{Bmatrix} = \begin{bmatrix} Q_{44} & 0 \\ 0 & Q_{55} \end{bmatrix} \begin{Bmatrix} \gamma_{yz} \\ \gamma_{zx} \end{Bmatrix} \quad (6b)$$

Where,  $(\sigma_x, \sigma_y, \tau_{xy}, \tau_{xz}, \tau_{yz})$  and  $(\varepsilon_x, \varepsilon_y, \gamma_{xy}, \gamma_{xz}, \gamma_{yz})$  represent the stress and strain components respectively. By utilizing the material properties described in Eq. (4), the stiffness coefficients denoted as  $Q_{ij}$  can be formulated as

$$Q_{11} = Q_{22} = \frac{E(z)}{1-\nu^2}, \quad (7a)$$

$$Q_{12} = \frac{\nu E(z)}{1-\nu^2}, \quad (7b)$$

$$Q_{44} = Q_{55} = Q_{66} = \frac{E(z)}{2(1+\nu)} \quad (7c)$$

### 2.3 Stability equations

The total potential energy of the functionally graded plate can be expressed as follows

$$U = \frac{1}{2} \int \int \int [\sigma_x(\varepsilon_x - \alpha T) + \sigma_y(\varepsilon_y - \alpha T) + \tau_{xy}\gamma_{xy} + \tau_{yz}\gamma_{yz} + \tau_{xz}\gamma_{xz}] dx dy dz \quad (8)$$

The principle of virtual work applicable to the current problem can be stated in the following manner

$$\int \int \left[ N_x \delta \varepsilon_x^0 + N_y \delta \varepsilon_y^0 + N_{xy} \delta \gamma_{xy}^0 + M_x^b \delta k_x^b + M_y^b \delta k_y^b + M_{xy}^b \delta k_{xy}^b + M_x^s \delta k_x^s \right. \\ \left. + M_y^s \delta k_y^s + M_{xy}^s \delta k_{xy}^s + S_{yz}^s \delta \gamma_{yz}^s + S_{xz}^s \delta \gamma_{xz}^s \right] dx dy = 0 \quad (9)$$

Where

$$\begin{Bmatrix} N_x & N_y & N_{xy} \\ M_x^b & M_y^b & M_{xy}^b \\ M_x^s & M_y^s & M_{xy}^s \end{Bmatrix} = \int_{-h/2}^{h/2} (\sigma_x, \sigma_y, \tau_{xy}) \begin{Bmatrix} 1 \\ z \\ f(z) \end{Bmatrix} dz \quad (10a)$$

$$(S_{xz}^s, S_{yz}^s) = \int_{-h/2}^{h/2} (\tau_{xz}, \tau_{yz}) g(z) dz \quad (10b)$$

By substituting Eq. (6) into Eq. (10), the stress resultants of the functionally graded plate can be connected to the total strains through the following relationship

$$\begin{Bmatrix} N \\ M^b \\ M^s \end{Bmatrix} = \begin{bmatrix} A & B & B^s \\ B & D & D^s \\ B^s & D^s & H^s \end{bmatrix} \begin{Bmatrix} \varepsilon \\ k^b \\ k^s \end{Bmatrix} - \begin{Bmatrix} N^T \\ M^{bT} \\ M^{sT} \end{Bmatrix}, \quad (11a)$$

$$S = A^s \gamma \quad (11b)$$

Where

$$N = \{N_x, N_y, N_{xy}\}^t, M^b = \{M_x^b, M_y^b, M_{xy}^b\}^t, M^s = \{M_x^s, M_y^s, M_{xy}^s\}^t, \quad (12a)$$

$$N^T = \{N_x^T, N_y^T, 0\}^t, M^{bT} = \{M_x^{bT}, M_y^{bT}, 0\}^t, M^{sT} = \{M_x^{sT}, M_y^{sT}, 0\}^t, \quad (12b)$$

$$\varepsilon = \{\varepsilon_x^0, \varepsilon_y^0, \gamma_{xy}^0\}^t, k^b = \{k_x^b, k_y^b, k_{xy}^b\}^t, k^s = \{k_x^s, k_y^s, k_{xy}^s\}^t, \quad (12c)$$

$$A = \begin{bmatrix} A_{11} & A_{12} & 0 \\ A_{12} & A_{22} & 0 \\ 0 & 0 & A_{66} \end{bmatrix}, B = \begin{bmatrix} B_{11} & B_{12} & 0 \\ B_{12} & B_{22} & 0 \\ 0 & 0 & B_{66} \end{bmatrix}, D = \begin{bmatrix} D_{11} & D_{12} & 0 \\ D_{12} & D_{22} & 0 \\ 0 & 0 & D_{66} \end{bmatrix} \quad (12d)$$

$$B^s = \begin{bmatrix} B_{11}^s & B_{12}^s & 0 \\ B_{12}^s & B_{22}^s & 0 \\ 0 & 0 & B_{66}^s \end{bmatrix}, D^s = \begin{bmatrix} D_{11}^s & D_{12}^s & 0 \\ D_{12}^s & D_{22}^s & 0 \\ 0 & 0 & D_{66}^s \end{bmatrix}, H^s = \begin{bmatrix} H_{11}^s & H_{12}^s & 0 \\ H_{12}^s & H_{22}^s & 0 \\ 0 & 0 & H_{66}^s \end{bmatrix} \quad (12e)$$

$$S = \{S_{xz}^s, S_{yz}^s\}^t, \gamma = \{\gamma_{xz}^s, \gamma_{yz}^s\}^t, A^s = \begin{bmatrix} A_{44}^s & 0 \\ 0 & A_{55}^s \end{bmatrix} \quad (12f)$$

Where  $A_{ij}$ ,  $B_{ij}$ , etc., represent the plate stiffness, defined as

$$\begin{Bmatrix} A_{11} B_{11} D_{11} B_{11}^s D_{11}^s H_{11}^s \\ A_{12} B_{12} D_{12} B_{12}^s D_{12}^s H_{12}^s \\ A_{66} B_{66} D_{66} B_{66}^s D_{66}^s H_{66}^s \end{Bmatrix} = \int_{-h/2}^{h/2} (1, z, z^2, f(z), zf(z), f^2(z)) \left\{ \begin{matrix} 1 \\ v^{(n)} \\ \frac{1-v^{(n)}}{2} \end{matrix} \right\} dz \quad (13a)$$

And

$$(A_{22}, B_{22}, D_{22}, B_{22}^s, D_{22}^s, H_{22}^s) = (A_{11}, B_{11}, D_{11}, B_{11}^s, D_{11}^s, H_{11}^s) \quad (13b)$$

$$A_{44}^s = A_{55}^s = \int_{-h/2}^{h/2} \frac{E(z)}{2(1-\nu)} [g(z)]^2 dz \quad (13c)$$

The stress and moment resultants, denoted as  $N_x^T = N_y^T$ ,  $M_x^{bT} = M_y^{bT}$  and  $M_x^{sT} = M_y^{sT}$ , resulting from thermal loading are defined as follows

$$\begin{Bmatrix} N_x^T \\ M_x^{bT} \\ M_x^{sT} \end{Bmatrix} = \int_{-h/2}^{h/2} \frac{E(z)}{1-\nu} \alpha(z) T \begin{Bmatrix} 1 \\ z \\ f(z) \end{Bmatrix} dz \quad (14)$$

The stability equations for the plate can be deduced through the criterion of adjacent equilibrium. Let's consider that the equilibrium condition of the functionally graded plate under thermal loads is described in relation to the displacement components  $(u_0^0, v_0^0, w_b^0, w_s^0)$ . The displacement components of a neighboring stable state deviate by  $(u_0^1, v_0^1, w_b^1, w_s^1)$  from the equilibrium position. Consequently, the complete displacements of this neighboring state are given by

$$u_0 = u_0^0 + u_0^1, v_0 = v_0^0 + v_0^1, w_b = w_b^0 + w_b^1, w_s = w_s^0 + w_s^1 \quad (15)$$

The superscript '1' denotes the stable state, and the superscript '0' represents the equilibrium condition.

By inserting Eqs. (2) and (15) into Eq. (9), and subsequently integrating by parts and then setting the coefficients of  $\delta u_0^1, \delta v_0^1, \delta w_b^1, \delta w_s^1$ , to zero independently, the governing stability

equations are derived for the theories involving shear deformation in the plate. These equations can be expressed as follows

$$\begin{aligned} \frac{\partial N_x^1}{\partial x} + \frac{\partial N_{xy}^1}{\partial y} &= 0 \\ \frac{\partial N_{xy}^1}{\partial x} + \frac{\partial N_y^1}{\partial y} &= 0 \\ \frac{\partial^2 M_x^{b1}}{\partial x^2} + 2 \frac{\partial^2 M_{xy}^{b1}}{\partial x \partial y} + \frac{\partial^2 M_y^{b1}}{\partial y^2} + \bar{N} &= 0 \\ \frac{\partial^2 M_x^{s1}}{\partial x^2} + 2 \frac{\partial^2 M_{xy}^{s1}}{\partial x \partial y} + \frac{\partial^2 M_y^{s1}}{\partial y^2} + \frac{\partial S_{xz}^{s1}}{\partial x} + \frac{\partial S_{yz}^{s1}}{\partial y} + \bar{N} &= 0 \end{aligned} \quad (16)$$

With

$$\bar{N} = \left[ N_x^0 \frac{\partial^2 (w_b^1 + w_s^1)}{\partial x^2} + N_y^0 \frac{\partial^2 (w_b^1 + w_s^1)}{\partial y^2} + 2N_{xy}^0 \frac{\partial^2 (w_b^1 + w_s^1)}{\partial x \partial y} \right] \quad (17)$$

The terms  $N_x^0$  and  $N_y^0$  represent the pre-buckling force resultants, which are determined as

$$N_x^0 = N_y^0 = - \int_{-h/2}^{h/2} \frac{\alpha(z)E(z)T}{1-\nu} dz. \quad (18)$$

### 3. Exact solution for a simply-supported FGM plate

Rectangular plates are typically categorized based on the type of support employed. In this context, our focus lies on obtaining the precise solution of Eq. (16) for a simply supported functionally graded (FG) plate. The subsequent boundary conditions are enforced at the lateral edges for the current four-variable refined plate theory

$$v_0^1 = w_b^1 = w_s^1 = \frac{\partial w_s^1}{\partial y} = N_x^1 = M_x^{b1} = M_x^{s1} = 0 \text{ at } x = 0, a, \quad (19a)$$

$$u_0^1 = w_b^1 = w_s^1 = \frac{\partial w_s^1}{\partial x} = N_y^1 = M_y^{b1} = M_y^{s1} = 0 \text{ at } y = 0, b. \quad (19b)$$

The subsequent approximate solution is observed to fulfill both the differential equation and the specified boundary conditions

$$\begin{Bmatrix} u_0^1 \\ v_0^1 \\ w_b^1 \\ w_s^1 \end{Bmatrix} = \sum_{m=1}^{\infty} \sum_{n=1}^{\infty} \begin{Bmatrix} U_{mn}^1 \cos(\lambda x) \sin(\mu y) \\ V_{mn}^1 \sin(\lambda x) \cos(\mu y) \\ W_{bmn}^1 \sin(\lambda x) \sin(\mu y) \\ W_{smn}^1 \sin(\lambda x) \sin(\mu y) \end{Bmatrix} \quad (20)$$

Where  $U_{mn}^1, V_{mn}^1, W_{bmn}^1$  and  $W_{smn}^1$  are arbitrary parameters to be determined,  $\lambda = m\pi/a$  and  $\mu = n\pi/b$  and  $m$  and  $n$  are mode numbers. Substituting Eq. (20) into Eq. (16), one obtains

$$[K]\{\Delta\} = \{P\} \quad (21)$$

Where  $\{\Delta\}$  denotes the column

$$\{\Delta\} = \{U_{mn}^1, V_{mn}^1, W_{bmn}^1, W_{smn}^1\}^t \quad (22)$$

And  $[K]$  is the symmetric matrix given by

$$[K] = \begin{bmatrix} a_{11} & a_{12} & a_{13} & a_{14} \\ a_{12} & a_{22} & a_{23} & a_{24} \\ a_{13} & a_{23} & a_{33} & a_{34} \\ a_{14} & a_{24} & a_{34} & a_{44} \end{bmatrix} \quad (23)$$

In order to obtain a nontrivial solution, the determinant of the coefficient matrix in Eq. (21) must equate to zero. This condition yields the thermal buckling load.

### 3.1 Buckling of FG plates under uniform temperature rise

The initial temperature of the plate is denoted as  $T_i$ . The temperature is then uniformly elevated to a final value  $T_f$ , at which point the plate undergoes buckling. This change in temperature is represented as  $\Delta T = T_f - T_i$ .

### 3.2 Buckling of FG plates subjected to graded temperature change across the thickness

It is assumed that the temperature at the upper surface is represented as  $T_t$ , and the temperature changes through the thickness in accordance with a power law distribution, reaching the lower surface temperature  $T_b$  at the point of buckling. In this context, the temperature gradient across the thickness is formulated as

$$T(z) = \Delta T \left( \frac{z}{h} + \frac{1}{2} \right)^\gamma + T_t \quad (24)$$

Where the buckling temperature difference  $\Delta T = T_t - T_b$  and  $\gamma$  is the temperature exponent ( $0 < \gamma < \infty$ ). Note that the value of  $\gamma$  equal to unity represents a linear temperature change across the thickness. While the value of  $\gamma$  excluding unity represents a non-linear temperature change through-the-thickness.

Where,  $\Delta T = T_t - T_b$  signifies the temperature difference at buckling, and  $\gamma$  represents the temperature exponent. It's noteworthy that a value of  $\gamma$  equal to unity indicates a linear temperature variation across the thickness. Conversely, a value of  $\gamma$  different from unity indicates a non-linear temperature change through the thickness.

## 4. Results

This research presents numerical results that illustrate the impact of temperature loads and different porosity distribution shapes on the critical loads of functionally graded plates under various thermal conditions. The analysis is conducted using the refined higher-order shear deformation plate theory. The material composition chosen for this study consists of a mixture of alumina ( $Al_2O_3$ ) and aluminum (Al). The Young's modulus for these materials is listed below:

$$E_m = 70 \text{ GPa}, \rho_m = 2702 \text{ kg/m}^3 \text{ ( "m" represents metal phase Al)},$$

$$E_c = 380 \text{ GPa}, \rho_c = 3800 \text{ kg/m}^3 \text{ ( c represents ceramic phase: } Al_2O_3 \text{)},$$

$$\text{Poisson ratio } \nu_m = \nu_c = 0.3.$$

Tables 1 and 2 provide a comprehensive analysis of the critical buckling load of an FGM plate subjected to uniform thermal loading. The power-law index is systematically varied, ranging from

Table 1 Effect of uniform porosity distribution on the critical load under uniform temperature variation of an FGM plate for different values of the power index and the  $a/b$  ratio ( $a/h=100, n=3$ )

$k$	Theories		$T_{cr}$			
			$a/b=1$	$a/b=2$	$a/b=3$	$a/b=5$
0	Tounsi (2020)	$\beta=0$	17.08	42.68	85.25	220.67
	Abdelhak (2015)	$\beta=0$	17.0895	42.6876	85.2551	220.6706
	Present	$\beta=0.1$	21.5075	53.7225	107.2939	277.7147
		$\beta=0.2$	29.0051	72.4514	144.6991	374.5327
1	Tounsi (2020)	$\beta=0$	7.94	19.83	39.62	102.63
	Abdelhak (2015)	$\beta=0$	7.9400	19.8359	39.6248	102.6356
	Present	$\beta=0.1$	8.7063	21.7510	43.4528	112.5694
		$\beta=0.2$	9.5975	23.9784	47.9061	124.1350
5	Tounsi (2020)	$\beta=0$	7.26	18.13	36.20	93.60
	Abdelhak (2015)	$\beta=0$	7.2607	18.1327	36.2025	93.6070
	Present	$\beta=0.1$	7.6555	19.1193	38.1736	98.7150
		$\beta=0.2$	7.4320	18.5630	37.0699	95.9169
10	Tounsi (2020)	$\beta=0$	7.46	18.63	37.20	96.12
	Abdelhak (2015)	$\beta=0$	7.4634	18.6367	37.2006	96.1214
	Present	$\beta=0.1$	8.2195	20.5231	40.9614	105.8006
		$\beta=0.2$	8.6722	21.6520	43.2096	111.5673

Table 2 Effect of uniform porosity distribution on the critical load under uniform temperature variation of an FGM plate for different values of the power index and the  $a/h$  ratio ( $n=3$ )

$k$	Theories		$T_{cr}$			
			$a/h=10$	$a/h=20$	$a/h=40$	$a/h=60$
0	Tounsi (2020)	$\beta=0$	1618.68	421.53	106.49	47.42
	Mahmoud <i>et al.</i> (2017)	$\beta=0$	1618.75	421.54	/	/
	Abdelhak (2015)	$\beta=0$	1618.682	421.535	106.494	47.423
	Refrafi (2020)	$\beta=0$	1594.16	396.57	/	/
	Present	$\beta=0$	1618.682	421.535	106.494	47.423
		$\beta=0.1$	2037.117	530.504	134.023	59.682
$\beta=0.2$		2747.304	715.450	180.747	80.489	
1	Tounsi (2020)	$\beta=0$	758.39	196.26	49.50	22.03
	Mahmoud <i>et al.</i> (2017)	$\beta=0$	758.42	196.27	/	/
	Abdelhak (2015)	$\beta=0$	758.396	196.265	49.502	49.502
	Refrafi (2020)	$\beta=0$	733.58	171.28	/	/
	Present	$\beta=0$	758.396	196.265	49.502	22.037
		$\beta=0.1$	833.237	215.314	54.285	24.165
$\beta=0.2$		921.074	237.518	59.851	26.640	
5	Tounsi (2020)	$\beta=0$	679.31	178.53	45.21	20.14
	Mahmoud <i>et al.</i> (2017)	$\beta=0$	679.72	178.56	/	/
	Abdelhak (2015)	$\beta=0$	679.3104	178.535	45.214	20.144
	Refrafi (2020)	$\beta=0$	653.77	153.50	/	/
	Present	$\beta=0$	679.3104	178.535	45.214	20.144
		$\beta=0.1$	717.2268215	188.310	47.677	21.240
$\beta=0.2$		701.1042513	183.132	46.302	20.622	

Table 2 Continued

10	Tounsi (2020)	$\beta=0$	692.69	183.14	46.45	20.70
	Mahmoud <i>et al.</i> (2017)	$\beta=0$	692.96	183.16	/	/
	Abdelhak (2015)	$\beta=0$	692.695	183.144	46.455	20.703
	Refrafi (2020)	$\beta=0$	667.57	158.14	/	/
	Present	$\beta=0$	692.695	183.144	46.455	20.703
		$\beta=0.1$	759.669	201.479	51.149	22.798
$\beta=0.2$		798.197	212.348	53.953	24.052	

Table 3 Effect of different forms of porosity distributions on the critical load of a square FGM plate under uniform temperature variation ( $a/h=10, k=5, a/b=1$ )

Porosity		$T_{cr}$				
		Distribution shape of porosity				
		Uniform Distribution	O Distribution	V Distribution	$\Lambda$ Distribution	X Distribution
$n=3$	$\beta=0$	679,3104	679,3104	679,3104	679,3104	679,3104
	$\beta=0.1$	717,2268	575,8735	744,5300	650,1290	742,1081
	$\beta=0.2$	701,1043	93,3162	823,8759	575,8735	782,3254
$n=5$	$\beta=0$	682,0146	682,0146	682,0146	682,0146	682,0146
	$\beta=0.1$	720,6190	577,9548	747,9908	652,7078	745,3811
	$\beta=0.2$	704,9511	93,2501	828,4844	577,9548	786,0169
$n=7$	$\beta=0$	684,1093	684,1093	684,1093	684,1093	684,1093
	$\beta=0.1$	723,0714	579,4928	750,5764	654,6541	747,9038
	$\beta=0.2$	707,4836	93,2316	831,7854	579,4928	788,8582
$n=9$	$\beta=0$	685,5861	685,5861	685,5861	685,5861	685,5861
	$\beta=0.1$	724,7623	580,5619	752,3784	656,0152	749,6794
	$\beta=0.2$	709,1732	93,2275	834,0538	580,5619	790,8576

Table 4 Effect of different forms of porosity distribution on the critical load  $T_{cr}$  of a square plate under three types of temperature variation ( $a/h=10, k=5, n=3$ )

Distribution shape of porosity	Porosity	$T_{cr}$		
		TemperatureUniform	TemperatureLinear	Temperature nonLinear
Uniform Distribution	$\beta=0$	679,3104	1159,9571	1595,4122
	$\beta=0.1$	717,2268	1170,4545	1575,1300
	$\beta=0.2$	701,1043	1056,1555	1372,9721
O-Distribution	$\beta=0$	679,3104	1159,9571	1595,4122
	$\beta=0.1$	575,8735	855,2427	1113,9740
	$\beta=0.2$	93,3162	110,0448	134,7991
V-Distribution	$\beta=0$	679,3104	1159,9571	1595,4122
	$\beta=0.1$	744,5300	1307,5459	1814,0381
	$\beta=0.2$	823,8759	1498,8965	2101,9707
$\Lambda$ -Distribution	$\beta=0$	679,3104	1159,9571	1595,4122
	$\beta=0.1$	650,1290	1040,4240	1393,7500
	$\beta=0.2$	575,8735	855,2427	1113,9740
X-Distribution	$\beta=0$	679,3104	1159,9571	1595,4122
	$\beta=0.1$	742,1081	1387,4803	1979,8573
	$\beta=0.2$	782,3254	1615,9818	2410,6365

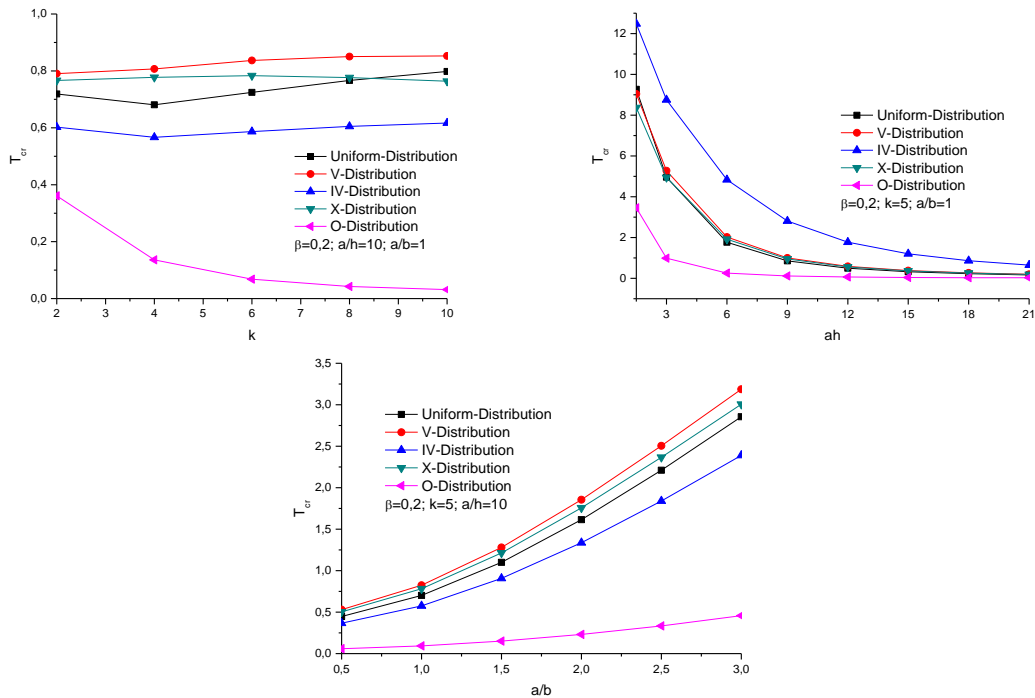


Fig. 2 Effect of porosity distribution shape on the critical load as a function of the power law index,  $a/b$  and  $a/h$  ratios for different porosity shapes under a uniform temperature variation ( $k = 5, a/b=1, a/h=10, \beta=0.2$ )

$k=0$  to 10, allowing for a thorough investigation of its influence. Additionally, the tables present the impact of the  $a/b$  and  $a/h$  ratios on the critical buckling load. The results clearly demonstrate a notable trend: an increasing  $a/b$  ratio leads to an enhanced critical buckling load. This finding underscores the importance of considering the geometric aspect ratio in optimizing the structural performance of FGM plates. However, it should be noted that as the FGM plate becomes thinner, the critical buckling load decreases. This observation emphasizes the need to carefully assess and balance the trade-off between plate thickness and buckling behavior when designing FGM structures.

The effect of variation in the pore distribution shape on the critical buckling load of a porous FGM plate for different values of  $n$  and different types of temperature loading is shown in Tables 3 and 4, respectively. The following parameters are considered:  $a/b=1, a/h=10$ , and  $k=5$ . The volumetric fraction of porosity is set as follows:  $\beta=0, 0.1$ , and  $0.2$ . From these results, it can be concluded that the variation in pore distribution shape has a significant effect on the critical buckling load. It can also be noted that a non-linear variation in temperature has a greater effect on the critical load compared to other types of variation.

Fig. 2 present the effect of porosity distribution shape on the critical load as a function of the power law index,  $a/b$  and  $a/h$  ratios for different porosity shapes under a uniform temperature variation. The volume fraction of porosity is taken  $\beta=0.2$ . Through this figure, it can be seen that the variation in the shape of the porosity distribution significantly influences the critical buckling load. The influence of the porosity distribution shape becomes more pronounced with increasing power index  $k$  and  $a/b$  ratio. However, it diminishes as the thickness ratio  $a/h$  increases.

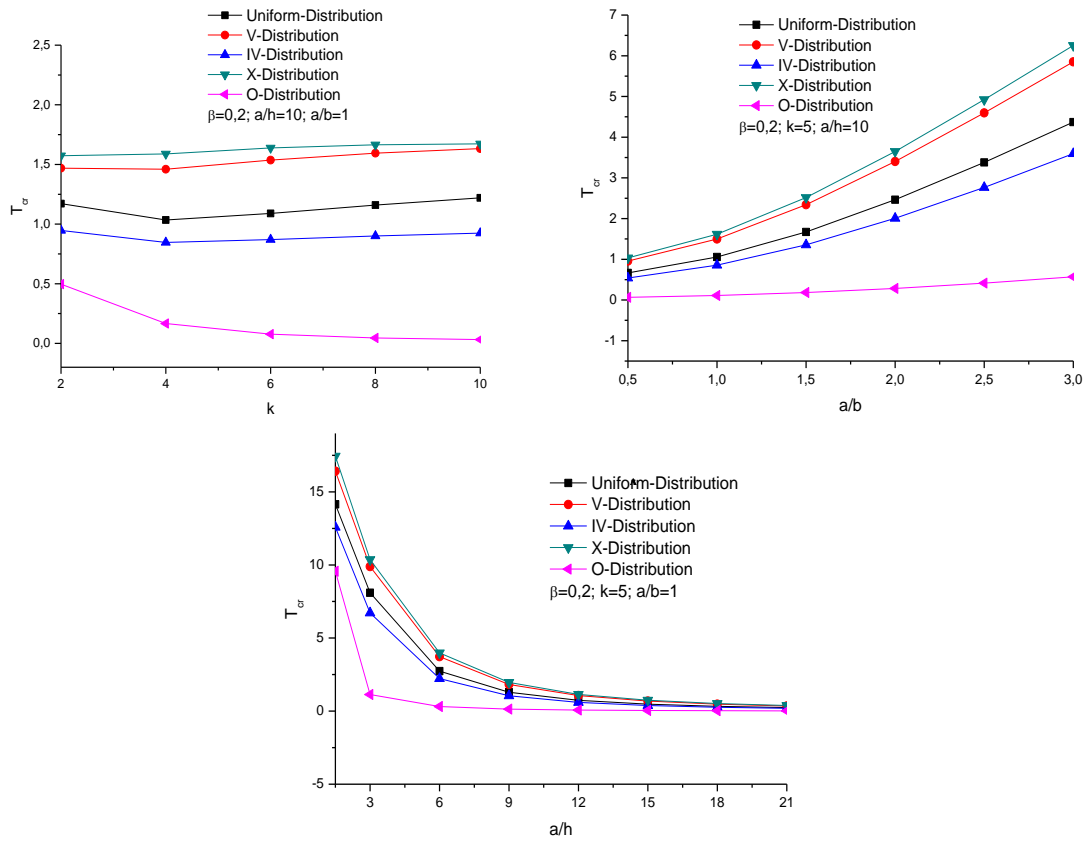


Fig. 3 Effect of porosity distribution shape on the critical load as a function of the power law index,  $a/b$  and  $a/h$  ratios for different porosity shapes under a linear temperature variation ( $k = 5$ ,  $a/b=1$ ,  $a/h=10$ ,  $\beta=0.2$ )

Figs. 3 and 4 present analyses on the impact of porosity distribution shape and thermal variations on the critical load of a Functionally Graded Material plate.

In Fig. 3, the research delves into the impact of porosity distribution shape on the critical load of the FGM plate, specifically under the influence of linear thermal loading. The analysis considers variations in the power index, as well as the ratios of  $a/b$  and  $a/h$ , while keeping the porosity ratio constant at a value of 0.2. The results of this analysis suggest that the porosity distribution has a notable influence on the behavior of the FGM plate under critical buckling conditions, especially when subjected to linear thermal loading. Variations in the power index,  $a/b$  ratio, and  $a/h$  ratio lead to significant fluctuations in the critical buckling load, highlighting the importance of considering the porosity distribution to ensure structural stability of the FGM plate under different scenarios. In Fig. 4, another analysis is conducted by introducing a non-linear thermal distribution. The results show that, in this case, the critical load becomes even more significant. This underscores the crucial importance of considering variations in the thermal distribution to accurately assess the critical buckling load of the FGM plate in real-world applications. By combining the information from both figures, a comprehensive understanding of the factors influencing the stability of the FGM plate under varying critical and thermal loads is obtained.

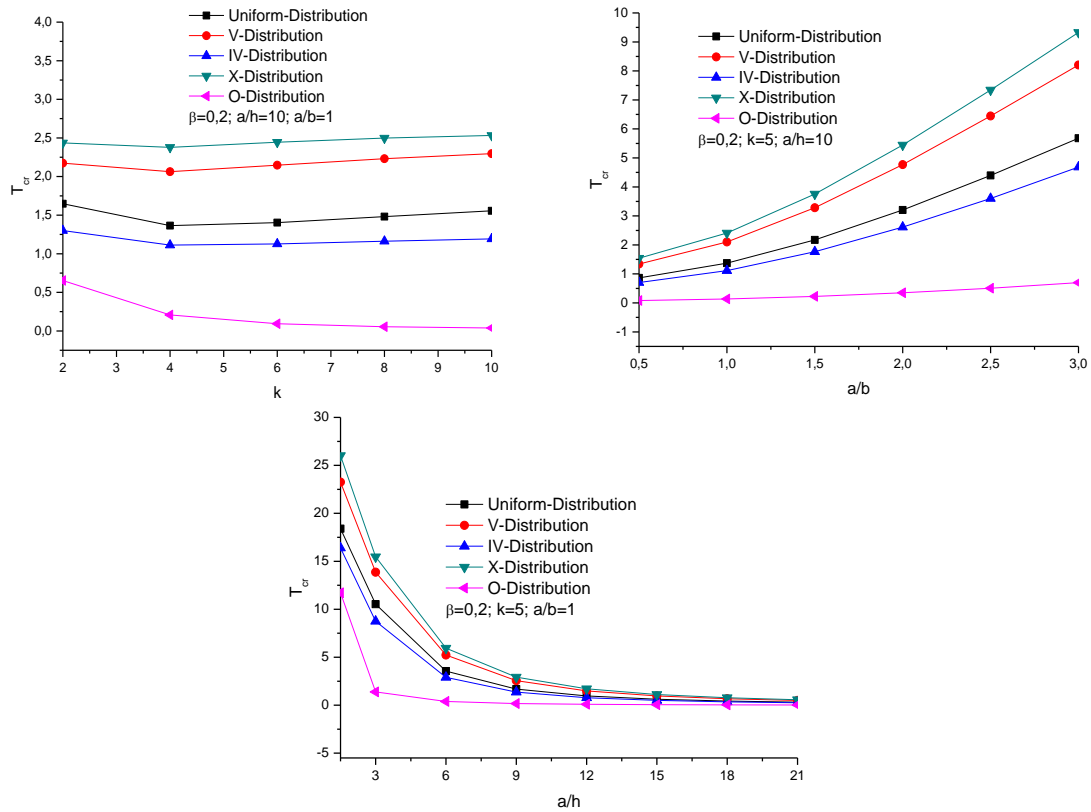


Fig. 4 Effect of porosity distribution shape on the critical load as a function of the power law index,  $a/b$  and  $a/h$  ratios for different porosity shapes under a non-linear temperature variation ( $k = 5$ ,  $a/b=1$ ,  $a/h=10$ ,  $\beta=0.2$ )

### 5. Conclusions

The thermal buckling behavior of FGM plates under various thermal loadings has been investigated in this study, employing a refined shear deformation plate theory. The material properties of the FGM exhibit variation along the thickness according to a modified power law formulation based on the volume fractions of the constituents. Additionally, a comprehensive parametric analysis of critical loading is conducted, considering factors such as power-law indexes, thickness ratios, aspect ratios, and parameters related to the distribution shape of porosity. This analysis highlights the following results on the influence of the thermal load:

1. The numerical results demonstrate that increasing the ratio  $a/h$  leads to a reduction in the critical load. Moreover, porous FG plates exhibit higher critical loads.
2. The findings confirm that the variation in the distribution shape of porosity has a significant impact on the critical load of the FGM plates.
3. Variations in power index,  $a/b$  ratio, and  $a/h$  ratio result in significant fluctuations in critical buckling load, highlighting the importance of considering porosity distribution to ensure structural stability of the FGM plate, under linear and non-linear thermal loading
4. The results obtained confirm that the variation in the shape of porosity distribution has a

significant impact on the critical load of FGM plates.

5. Finally, it is very important to emphasize the crucial importance of taking into account variations in thermal distribution to accurately evaluate the critical buckling load of the FGM plate in real applications. By combining the information from the two figures, a comprehensive understanding of the factors influencing the stability of the FGM plate under various critical and thermal loads is obtained.

## Acknowledgments

This research was supported by the Algerian Ministry of Higher Education and Scientific Research (MESRS) as part of the grant for the PRFU research project n° A01L02UN140120200002 and by the University of Tiaret, in Algeria.

## References

- Abdelhak, Z., Hadji, L., Daouadji, T.H. and Bedia, E.A. (2015), "Thermal buckling of functionally graded plates using a n-order four variable refined theory", *Adv. Mater. Res.*, **4**(1), 31. <http://doi.org/10.12989/amr.2015.4.1.31>.
- Abderezak, R., Daouadji, T.H. and Rabia, B. (2020), "Analysis of interfacial stresses of the reinforced concrete foundation beams repairing with composite materials plate", *Couple. Syst. Mech.*, **9**(5), 473. <http://doi.org/10.12989/csm.2020.9.5.473>.
- Abderezak, R., Daouadji, T.H. and Rabia, B. (2021), "Aluminum beam reinforced by externally bonded composite materials", *Adv. Mater. Res.*, **10**(1), 23. <http://doi.org/10.12989/amr.2021.10.1.023>.
- Abderezak, R., Daouadji, T.H. and Rabia, B. (2021), "Fiber reinforced polymer in civil engineering: Shear lag effect on damaged RC cantilever beams bonded by prestressed plate", *Couple. Syst. Mech.*, **10**(4), 299-316. <http://doi.org/10.12989/csm.2021.10.4.299>.
- Abderezak, R., Daouadji, T.H. and Rabia, B. (2021), "Modeling and analysis of the imperfect FGM-damaged RC hybrid beams", *Adv. Comput. Des.*, **6**(2), 117. <http://doi.org/10.12989/acd.2021.6.2.117>.
- Abderezak, R., Daouadji, T.H. and Rabia, B. (2021), "New solution for damaged porous RC cantilever beams strengthening by composite plate", *Adv. Mater. Res.*, **10**(3), 169. <http://doi.org/10.12989/amr.2021.10.3.169>.
- Abderezak, R., Daouadji, T.H. and Rabia, B. (2022), "Analysis and modeling of hyperstatic RC beam bonded by composite plate symmetrically loaded and supported", *Steel Compos. Struct.*, **45**(4), 591-603. <https://doi.org/10.12989/scs.2022.45.4.591>.
- Abderezak, R., Daouadji, T.H. and Tayeb, B. (2023), "Composite aluminum-slab RC beam bonded by a prestressed hybrid carbon-glass composite material", *Struct. Eng. Mech.*, **85**(5), 573. <https://doi.org/10.12989/sem.2023.85.5.573>.
- Abderezak, R., Rabia, B. and Daouadji, T.H. (2022), "Rehabilitation of RC structural elements: Application for continuous beams bonded by composite plate under a prestressing force", *Adv. Mater. Res.*, **11**(2), 91-109. <https://doi.org/10.12989/amr.2022.11.2.091>.
- Abderezak, R., Rabia, B., Daouadji, T.H., Abbes, B., Belkacem, A. and Abbes, F. (2018), "Elastic analysis of interfacial stresses in prestressed PFGM-RC hybrid beams", *Adv. Mater. Res.*, **7**(2), 83. <https://doi.org/10.12989/amr.2018.7.2.083>.
- Aicha, K., Rabia, B., Daouadji, T.H. and Bouzidene, A. (2020), "Effect of porosity distribution rate for bending analysis of imperfect FGM plates resting on Winkler-Pasternak foundations under various boundary conditions", *Couple. Syst. Mech.*, **9**(6), 575. <http://doi.org/10.12989/csm.2020.9.6.575>.
- Aissa, B., Rabia, B. and Tahar, H.D. (2023), "Predicting and analysis of interfacial stress distribution in RC

- beams strengthened with composite sheet using artificial neural network”, *Struct. Eng. Mech.*, **87**(6), 517-527. <https://doi.org/10.12989/sem.2023.87.6.517>.
- Alashkar, A., Elkafrawy, M., Hawileh, R. and AlHamaydeh, M. (2022), “Buckling analysis of functionally graded materials (FGM) thin plates with various circular cutout arrangements”, *J. Compos. Sci.*, **6**(9), 277. <https://doi.org/10.3390/jcs6090277>.
- Benferhat, R., Daouadji, T.H. and Mansour, M.S. (2016), “Free vibration analysis of FG plates resting on an elastic foundation and based on the neutral surface concept using higher-order shear deformation theory”, *Comptes Rendus Mecanique*, **344**(9), 631-641. <https://doi.org/10.1016/j.crme.2016.03.002>.
- Bouakaz, K., Daouadji, T.H., Meftah, S.A., Ameer, M., Tounsi, A. and Bedia, E.A. (2014), “A numerical analysis of steel beams strengthened with composite materials”, *Mech. Compos. Mater.*, **50**, 491-500. <https://doi.org/10.1007/s11029-014-9435-x>.
- Bouiadjra, M.B., Ahmed Houari, M.S. and Tounsi, A. (2012), “Thermal buckling of functionally graded plates according to a four-variable refined plate theory”, *J. Therm. Stress.*, **35**(8), 677-694. <http://doi.org/10.1080/01495739.2012.688665>.
- Bourada, F., Bousahla, A.A., Tounsi, A., Tounsi, A., Tahir, S.I., Al-Osta, M.A. and Do-Van, T. (2023), “An integral quasi-3D computational model for the hygro-thermal wave propagation of imperfect FGM sandwich plates”, *Comput. Concrete*, **32**(1), 61-74. <https://doi.org/10.12989/cac.2023.32.1.061>.
- Bouaid, H., Rabia, B. and Daouadji, T.H. (2022), “Curvature ductility of confined HSC columns”, *International Conference on Innovative Solutions in Hydropower Engineering and Civil Engineering*, Singapore, September.
- Bouaid, H., Rabia, B. and Daouadji, T.H. (2023), “Ultimate behavior of RC beams strengthened in flexure using FRP material”, *Eng. Struct.*, **289**, 116300. <https://doi.org/10.1016/j.engstruct.2023.116300>.
- Chen, D., Yang, J. and Kitipornchai, S. (2015), “Elastic buckling and static bending of shear deformable functionally graded porous beam”, *Compos. Struct.*, **133**, 54-61. <https://doi.org/10.1016/j.compstruct.2015.07.052>.
- Chergui, S., Daouadji, T.H., Hamrat, M., Boulekbache, B., Bougara, A., Abbes, B. and Amziane, S. (2019), “Interfacial stresses in damaged RC beams strengthened by externally bonded prestressed GFRP laminate plate: Analytical and numerical study”, *Adv. Mater. Res.*, **8**(3), 197. <https://doi.org/10.12989/amr.2019.8.3.197>.
- Daouadji, T.H. (2013), “Analytical analysis of the interfacial stress in damaged reinforced concrete beams strengthened by bonded composite plates”, *Strength Mater.*, **45**(5), 587-597. <https://doi.org/10.1007/s11223-013-9496-4>.
- Daouadji, T.H. (2017), “Analytical and numerical modeling of interfacial stresses in beams bonded with a thin plate”, *Adv. Comput. Des.*, **2**(1), 57-69. <https://doi.org/10.12989/acd.2017.2.1.057>.
- Daouadji, T.H., Abderezak, R. and Rabia, B. (2022), “New technique for repairing circular steel beams by FRP plate”, *Adv. Mater. Res.*, **11**(3), 171-190. <https://doi.org/10.12989/amr.2022.11.3.171>.
- Daouadji, T.H., Abderezak, R., Rabia, B. and Tounsi, A. (2021), “Renovation of steel beams using by imperfect functionally graded materials plate”, *Steel Compos. Struct.*, **41**(6), 851-860. <https://doi.org/10.12989/scs.2021.41.6.851>.
- Fan, F., Safaei, B. and Sahmani, S. (2021), “Buckling and postbuckling response of nonlocal strain gradient porous functionally graded micro/nano-plates via NURBS-based isogeometric analysis”, *Thin Wall. Struct.*, **159**, 107231. <https://doi.org/10.1016/j.tws.2020.107231>.
- Hadj, B., Rabia, B. and Daouadji, T.H. (2021), “Vibration analysis of porous FGM plate resting on elastic foundations: effect of the distribution shape of porosity”, *Couple. Syst. Mech.*, **10**(1), 61. <http://doi.org/10.12989/csm.2021.10.1.061>.
- Hamrat, M., Bouziadi, F., Boulekbache, B., Daouadji, T.H., Chergui, S., Labed, A. and Amziane, S. (2020), “Experimental and numerical investigation on the deflection behavior of pre-cracked and repaired reinforced concrete beams with fiber-reinforced polymer”, *Constr. Build. Mater.*, **249**, 118745. <https://doi.org/10.1016/j.conbuildmat.2020.118745>.
- Hashim, H.A. and Sadiq, I.A. (2021), “A five-variable refined plate theory for thermal buckling analysis of composite plates”, *Compos. Mater. Eng.*, **3**(2), 135-155. <http://doi.org/10.12989/cme.2021.3.2.135>.

- Henni, M.A.B., Abbès, B., Daouadji, T.H., Abbès, F. and Adim, B. (2021), "Numerical modeling of hygrothermal effect on the dynamic behavior of hybrid composite plates", *Steel Compos. Struct.*, **39**(6), 751-763. <http://doi.org/10.12989/scs.2021.39.6.751>.
- Kablia, A., Benferhat, R. and Hassaine Daouadji, T. (2022), "Dynamic of behavior for imperfect FGM plates resting on elastic foundation containing various distribution rates of porosity: Analysis and modeling", *Couple. Syst. Mech.*, **11**(5), 389-409. <https://doi.org/10.12989/csm.2022.11.5.389>.
- Kablia, A., Benferhat, R., Daouadji, T.H. and Abderezak, R. (2023), "Free vibration of various types of FGP sandwich plates with variation in porosity distribution", *Struct. Eng. Mech.*, **85**(1), 1-14. <https://doi.org/10.12989/sem.2023.85.1.00>.
- Kumar, V., Singh, S.J., Saran, V.H. and Harsha, S.P. (2023, September), "Effect of elastic foundation and porosity on buckling response of linearly varying functionally graded material plate", *Struct.*, **55**, 1186-1203. <https://doi.org/10.1016/j.istruc.2023.06.084>.
- Mahmoud, S.R. and Tounsi, A. (2017), "A new shear deformation plate theory with stretching effect for buckling analysis of functionally graded sandwich plates", *Steel Compos. Struct.*, **24**(5), 569-578. <https://doi.org/10.12989/scs.2017.24.5.569>.
- Mokhtar, B., Abdelouahed, T., Abbas, A. and Abdalkader, M. (2009), "Buckling analysis of functionally graded plates with simply supported edges", *Leonardo J. Sci.*, **16**, 21-32.
- Rabia, B., Abderezak, R., Daouadji, T.H., Abbes, B., Belkacem, A. and Abbes, F. (2018), "Analytical analysis of the interfacial shear stress in RC beams strengthened with prestressed exponentially-varying properties plate", *Adv. Mater. Res.*, **7**(1), 29. <https://doi.org/10.12989/amr.2018.7.1.029>.
- Rabia, B., Daouadji, T.H. and Abderezak, R. (2019), "Effect of distribution shape of the porosity on the interfacial stresses of the FGM beam strengthened with FRP plate", *Earthq. Struct.*, **16**(5), 601. <https://doi.org/10.12989/eas.2019.16.5.601>.
- Rabia, B., Daouadji, T.H. and Abderezak, R. (2019), "Effect of porosity in interfacial stress analysis of perfect FGM beams reinforced with a porous functionally graded materials plate", *Struct. Eng. Mech.*, **72**(3), 293-304. <https://doi.org/10.12989/sem.2019.72.3.293>.
- Rabia, B., Daouadji, T.H. and Abderezak, R. (2020), "Predictions of the maximum plate end stresses of imperfect FRP strengthened RC beams: Study and analysis", *Adv. Mater. Res.*, **9**(4), 265. <http://doi.org/10.12989/amr.2020.9.4.265>.
- Rabia, B., Daouadji, T.H. and Abderezak, R. (2021), "Analysis and sizing of RC beams reinforced by external bonding of imperfect functionally graded plate", *Adv. Mater. Res.*, **10**, 77-98. <http://doi.org/10.12989/amr.2021.10.2.077>.
- Rabia, B., Daouadji, T.H. and Abderezak, R. (2021), "Effect of air bubbles in concrete on the mechanical behavior of RC beams strengthened in flexion by externally bonded FRP plates under uniformly distributed loading", *Compos. Mater. Eng.*, **3**(1), 41. <http://doi.org/10.12989/cme.2021.3.1.041>.
- Rabia, B., Daouadji, T.H. and Abderezak, R. (2023), "Mechanical behavior of RC beams bonded with thin porous FGM plates: Case of fiber concretes based on local materials from the mountains of the Tiaret highlands", *Couple. Syst. Mech.*, **12**(3), 241-260. <https://doi.org/10.12989/csm.2023.12.3.241>.
- Radwan, A.F. (2019), "Effects of non-linear hygrothermal conditions on the buckling of FG sandwich plates resting on elastic foundations using a hyperbolic shear deformation theory", *J. Sandw. Struct. Mater.*, **21**(1), 289-319. <https://doi.org/10.1177/1099636217693557>.
- Ramu, I. and Mohanty, S.C. (2014), "Buckling analysis of rectangular functionally graded material plates under uniaxial and biaxial compression load", *Procedia Eng.*, **86**, 748-757. <https://doi.org/10.1016/j.proeng.2014.11.094>.
- Reddy, B.S., Kumar, J.S., Reddy, C.E. and Reddy, K. (2013), "Buckling analysis of functionally graded material plates using higher order shear deformation theory", *J. Compos.*, **2013**, Article ID 808764. <https://doi.org/10.1155/2013/808764>.
- Refrafi, S., Bousahla, A.A., Bouhadra, A., Menasria, A., Bourada, F., Tounsi, A., ... & Tounsi, A. (2020), "Effects of hygro-thermo-mechanical conditions on the buckling of FG sandwich plates resting on elastic foundations", *Comput. Concrete*, **25**(4), 311-325. <https://doi.org/10.12989/cac.2020.25.4.311>.
- Sitli, Y., Mhada, K., Bourihane, O. and Rhanim, H. (2021), "Buckling and post-buckling analysis of a

- functionally graded material (FGM) plate by the asymptotic numerical method”, *Struct.*, **31**, 1031-1040. <https://doi.org/10.1016/j.istruc.2021.01.100>.
- Tahar, H.D., Abderezak, R. and Rabia, B. (2020), “Flexural performance of wooden beams strengthened by composite plate”, *Struct. Monit. Mainten.*, **7**(3), 233-259. <http://doi.org/10.12989/smm.2020.7.3.233>.
- Tahar, H.D., Abderezak, R. and Rabia, B. (2021), “A new model for adhesive shear stress in damaged RC cantilever beam strengthened by composite plate taking into account the effect of creep and shrinkage”, *Struct. Eng. Mech.*, **79**(5), 531. <http://doi.org/10.12989/sem.2021.79.5.531>.
- Tahar, H.D., Abderezak, R. and Rabia, B. (2021), “Hyperstatic steel structure strengthened with prestressed carbon/glass hybrid laminated plate”, *Couple. Syst. Mech.*, **10**(5), 393-414. <https://doi.org/10.12989/csm.2021.10.5.393>.
- Tahar, H.D., Abderezak, R., Rabia, B. and Tounsi, A. (2021), “Impact of thermal effects in FRP-RC hybrid cantilever beams”, *Struct. Eng. Mech.*, **78**(5), 573-583. <http://doi.org/10.12989/sem.2021.78.5.573>.
- Tahar, H.D., Abderezak, R., Rabia, B. and Tounsi, A. (2021), “Performance of damaged RC continuous beams strengthened by prestressed laminates plate: Impact of mechanical and thermal properties on interfacial stresses”, *Couple. Syst. Mech.*, **10**(2), 161-184. <http://doi.org/10.12989/csm.2021.10.2.161>.
- Tahar, H.D., Boussad, A., Abderezak, R., Rabia, B., Fazilay, A. and Belkacem, A. (2019), “Flexural behaviour of steel beams reinforced by carbon fibre reinforced polymer: Experimental and numerical study”, *Struct. Eng. Mech.*, **72**(4), 409-420. <https://doi.org/10.12989/sem.2019.72.4.409>.
- Thinh, T.I., Tu, T.M., Quoc, T.H. and Long, N.V. (2016), “Vibration and buckling analysis of functionally graded plates using new eight-unknown higher order shear deformation theory”, *Lat. Am. J. Solid. Struct.*, **13**, 456-477. <https://doi.org/10.1590/1679-78252522>.
- Tlidji, Y., Benferhat, R., Daouadji, T.H., Tounsi, A. and Trinh, L.C. (2022), “Free vibration analysis of FGP nanobeams with classical and non-classical boundary conditions using State-space approach”, *Adv. Nano Res.*, **13**(5), 453. <https://doi.org/10.12989/anr.2022.13.5.453>.
- Tounsi, A., Al-Dulaijan, S.U., Al-Osta, M.A., Chikh, A., Al-Zahrani, M.M., Sharif, A. and Tounsi, A. (2020), “A four variable trigonometric integral plate theory for hygro-thermo-mechanical bending analysis of AFG ceramic-metal plates resting on a two-parameter elastic foundation”, *Steel Compos. Struct.*, **34**(4), 511-524. <https://doi.org/10.12989/scs.2020.34.4.511>.
- Tounsi, A., Daouadji, T.H. and Benyoucef, S. (2009), “Interfacial stresses in FRP-plated RC beams: Effect of adherend shear deformations”, *Int. J. Adhes. Adhesiv.*, **29**(4), 343-351. <https://doi.org/10.1016/j.ijadhadh.2008.06.008>.
- Wang, J.F., Cao, S.H. and Zhang, W. (2021), “Thermal vibration and buckling analysis of functionally graded carbon nanotube reinforced composite quadrilateral plate”, *Eur. J. Mech.-A/Solid.*, **85**, 104105. <https://doi.org/10.1016/j.euromechsol.2020.104105>.
- Zenkour, A.M. and Aljadani, M.H. (2022), “Buckling response of functionally graded porous plates due to a quasi-3D refined theory”, *Math.*, **10**(4), 565. <https://doi.org/10.3390/math10040565>.
- Zghal, S., Trabelsi, S. and Dammak, F. (2021), “Thermomechanical buckling of FGM skew plate”, *International Conference Design and Modeling of Mechanical Systems*, Cham, December. <https://doi.org/10.1007/978-3-031-14615-2-10>.
- Zohra, A., Rabia, B. and Tahar, H.D. (2023), “Critical thermal buckling analysis of porous FGP sandwich plates under various boundary conditions”, *Struct. Eng. Mech.*, **87**(1), 29-46. <https://doi.org/10.12989/sem.2023.87.1.029>.